

# The Helicity Sign of Flux Transfer Event Flux Ropes and its Relationship to the Guide Field and Hall Physics in Magnetic Reconnection at the Magnetopause

Souhail Dahani<sup>1</sup>, Rungployphan Kieokaew<sup>2</sup>, Vincent Génot<sup>3</sup>, Benoit Lavraud<sup>4</sup>, Yuxi Chen<sup>5</sup>, Bayane Michotte de Welle<sup>6</sup>, Nicolas Aunai<sup>7</sup>, Gábor Tóth<sup>8</sup>, Paul A Cassak<sup>9</sup>, Naïs Fargette<sup>2</sup>, Robert C Fear<sup>10</sup>, Aurelie Marchaudon<sup>11</sup>, Daniel J Gershman<sup>12</sup>, Barbara L. Giles<sup>12</sup>, Roy B. Torbert<sup>13</sup>, and Burch Jim<sup>14</sup>

<sup>1</sup>Institut de Recherche en Astrophysique et Planétologie, CNRS, UPS, CNES, Université de Toulouse

<sup>2</sup>Institut de Recherche en Astrophysique et Planétologie

<sup>3</sup>IRAP

<sup>4</sup>Institut de Recherche en Astrophysique et Planetologie - CNRS

<sup>5</sup>University of Michigan-Ann Arbor

<sup>6</sup>Laboratory of Plasma Physics, CNRS, Ecole Polytechnique, UPMC, Université Paris Sud

<sup>7</sup>IRAP, Toulouse, France

<sup>8</sup>Department of Climate and Space Sciences and Engineering, University of Michigan

<sup>9</sup>West Virginia University

<sup>10</sup>University of Southampton

<sup>11</sup>Institut de Recherche en Astrophysique et Planétologie, CNRS, CNES et Université Paul Sabatier

<sup>12</sup>NASA Goddard Space Flight Center

<sup>13</sup>University of New Hampshire

<sup>14</sup>Southwest Research Institute

November 22, 2022

## Abstract

Flux Transfer Events (FTEs) are transient magnetic flux ropes typically found at the Earth's magnetopause on the dayside. While it is known that FTEs are generated by magnetic reconnection, it remains unclear how the details of magnetic reconnection controls their properties. A recent study showed that the helicity sign of FTEs positively correlates with the east-west ( $B_y$ ) component of the Interplanetary Magnetic Field (IMF). With data from the Cluster and Magnetospheric Multiscale missions, we performed a statistical study of 166 quasi force-free FTEs. We focus on their helicity sign and possible association with upstream solar wind conditions and local magnetic reconnection properties. Using both in situ data and magnetic shear modeling, we find that FTEs whose helicity sign corresponds to the IMF  $B_y$  are associated with moderate magnetic shears while those that does not correspond to the IMF  $B_y$  are associated with higher magnetic shears. While uncertainty in IMF propagation to the magnetopause may lead to randomness in the determination of the flux rope core field and helicity, we rather propose that for small IMF  $B_y$ , which corresponds to high shear and low guide field, the Hall pattern of magnetic reconnection determines the FTE core field and helicity sign. In that context we explain how the temporal sequence of multiple X-line formation and the reconnection rate are important in determining the flux rope helicity sign. This work highlights a fundamental connection

between kinetic processes at work in magnetic reconnection and the macroscale structure of FTEs.

# The Helicity Sign of Flux Transfer Event Flux Ropes and its Relationship to the Guide Field and Hall Physics in Magnetic Reconnection at the Magnetopause

S. Dahani <sup>1</sup>, R. Kieokaew <sup>1</sup>, V. Génot <sup>1</sup>, B. Lavraud <sup>1,2</sup>, Y. Chen <sup>3</sup>, B.  
Michotte de Welle <sup>4</sup>, N. Aunai <sup>4</sup>, G. Tóth <sup>5</sup>, P. A. Cassak <sup>6</sup>, N. Fargette <sup>1</sup>, R.  
C. Fear <sup>7</sup>, A. Marchaudon <sup>1</sup>, D. Gershman <sup>8</sup>, B. Giles <sup>8</sup>, R. Torbert <sup>9</sup>, J.  
Burch <sup>10</sup>

<sup>1</sup>Institut de Recherche en Astrophysique et Planétologie, CNRS, UPS, CNES, Université de Toulouse,  
Toulouse, France

<sup>2</sup>Laboratoire d'Astrophysique de Bordeaux, Univ. Bordeaux, CNRS, Pessac, France

<sup>3</sup>Department of Astrophysical Sciences and Princeton Plasma Physics Laboratory, Princeton University,  
Princeton, NJ 08540, USA

<sup>4</sup>Laboratory of Plasma Physics, CNRS, Ecole Polytechnique, UPMC, Université Paris Sud, Orsay, France

<sup>5</sup>Department of Climate and Space Sciences and Engineering, University of Michigan, Ann Arbor, MI,  
USA

<sup>6</sup>Department of Physics and Astronomy and center for KINETIC Plasma Physics, West Virginia  
University, Morgantown, WV, USA

<sup>7</sup>School of Physics & Astronomy, University of Southampton, Southampton, UK

<sup>8</sup>NASA Goddard Space Flight Center, Greenbelt, MD, USA

<sup>9</sup>Space Science Center, University of New Hampshire, Durham, NH, USA

<sup>10</sup>Southwest Research Institute, San Antonio, TX, USA

## Key Points:

- We study the helicity sign of Flux Transfer Events and investigate upstream solar wind conditions and local magnetic shear around them.
- The helicity sign is found to be unassociated to the Interplanetary Magnetic Field (BY) component when the local magnetic shear is high.
- The FTEs' helicity sign in such cases may relate to the Hall field of magnetic reconnection in the absence of a guide field.

---

Corresponding author: Souhail Dahani, [sdahani@irap.omp.eu](mailto:sdahani@irap.omp.eu)

30 **Abstract**

31 Flux Transfer Events (FTEs) are transient magnetic flux ropes typically found at the  
 32 Earth’s magnetopause on the dayside. While it is known that FTEs are generated by  
 33 magnetic reconnection, it remains unclear how the details of magnetic reconnection con-  
 34 trols their properties. A recent study showed that the helicity sign of FTEs positively  
 35 correlates with the east-west ( $B_y$ ) component of the Interplanetary Magnetic Field (IMF).  
 36 With data from the Cluster and Magnetospheric Multiscale missions, we performed a  
 37 statistical study of 166 quasi force-free FTEs. We focus on their helicity sign and pos-  
 38 sible association with upstream solar wind conditions and local magnetic reconnection  
 39 properties. Using both in situ data and magnetic shear modeling, we find that FTEs whose  
 40 helicity sign corresponds to the IMF  $B_y$  are associated with moderate magnetic shears  
 41 while those that does not correspond to the IMF  $B_y$  are associated with higher magnetic  
 42 shears. While uncertainty in IMF propagation to the magnetopause may lead to random-  
 43 ness in the determination of the flux rope core field and helicity, we rather propose that  
 44 for small IMF  $B_y$ , which corresponds to high shear and low guide field, the Hall pattern  
 45 of magnetic reconnection determines the FTE core field and helicity sign. In that con-  
 46 text we explain how the temporal sequence of multiple X-line formation and the recon-  
 47 nection rate are important in determining the flux rope helicity sign. This work high-  
 48 lights a fundamental connection between kinetic processes at work in magnetic recon-  
 49 nection and the macroscale structure of FTEs.

50 **Plain Language Summary**

51 In the vicinity of the Earth’s magnetosphere outer boundary, the magnetopause,  
 52 twisted magnetic field structures known as “Flux Transfer Events” (FTEs) are often de-  
 53 tected by spacecraft in-situ. They temporarily connect the solar wind to the Earth’s iono-  
 54 sphere, allowing the transfer of solar wind flux into the magnetosphere. It is known that  
 55 FTEs are produced as a consequence of magnetic reconnection, a process that rearranges  
 56 the topology of sheared magnetic fields, between the shocked solar wind and the geomag-  
 57 netic field. However, our understanding of how the microphysics of magnetic reconnec-  
 58 tion can lead to the macroscopic structures of FTEs is still limited. We revisit the in-  
 59 situ observations of FTEs made by the Cluster and Magnetospheric Multiscale missions.  
 60 We focus on the twist feature of FTEs as characterized by their helicity and investigate  
 61 its relationship to solar wind conditions and possible link to magnetic reconnection prop-

62 erities. By investigating local magnetic shear conditions around FTE locations, we found  
 63 that the FTE helicity is determined by a kinetic feature of magnetic reconnection known  
 64 as the “Hall magnetic field”. Our study highlights a close connection between a kinetic  
 65 process of magnetic reconnection and the global structure FTEs, constituting a cross-  
 66 scale coupling effect in solar-terrestrial interaction.

## 67 1 Introduction

68 Flux Transfer Events (FTEs) are magnetic flux ropes produced at the dayside mag-  
 69 netopause as a consequence of magnetic reconnection. They were first observed by Russell  
 70 and Elphic (1978) using magnetic field measurement from ISEE 1 and 2. An FTE is recog-  
 71 nised in in-situ spacecraft time-series data as a bipolar variation in the magnetic field  
 72 component normal to the magnetopause (*i.e.*, magnetic field  $B_N$ ). The bipolar signa-  
 73 ture consists of a variation of the magnetic field from positive to negative or negative to  
 74 positive as reported by Russell and Elphic (1979) and Rijnbeek et al. (1982). The bipo-  
 75 lar signature is typically co-located with an enhancement in the magnetic field strength  
 76 compared to the ambient field (Paschmann et al., 1982). Various mechanisms were sug-  
 77 gested to explain the formation of FTEs. Lee and Fu (1985) proposed that an FTE is  
 78 created between two reconnection X-lines formed simultaneously on the dayside mag-  
 79 netopause. Using global magnetohydrodynamics (MHD) simulations, Raeder (2006) showed  
 80 that FTEs can be generated by sequential, magnetic reconnection where reconnection  
 81 X-lines are formed one after the other under a large dipole tilt condition (*e.g.*, during  
 82 the winter/summer season on the Northern/Southern hemisphere); Dorelli and Bhattachar-  
 83 jee (2009) later showed that the dipole tilt is not required to produce FTEs. Other for-  
 84 mation mechanisms were also proposed based on single X-line reconnection due to the  
 85 nature of unsteady or transient reconnection (*e.g.*, Southwood et al., 1988; Scholer, 1988).  
 86 To date, there are many studies that support the FTEs generation due to multiple X-  
 87 line reconnection (*e.g.*, Hasegawa et al., 2010; Øieroset et al., 2011; Kieokaew et al., 2021).

An FTE flux rope has a helical, twisted interior (*e.g.*, Russell & Elphic, 1979; Cow-  
 ley, 1982; Saunders et al., 1984). We can characterize this property using the magnetic  
 helicity, which is defined as,

$$\mathcal{H} = \int_V \mathbf{A} \cdot \mathbf{B} dV, \quad (1)$$

88 where  $\mathbf{A}$  is the magnetic vector potential,  $\mathbf{B}$  is the magnetic field, and  $V$  is the integra-  
 89 tion volume. Magnetic helicity has been used to characterize the geometrical features

(such as kinking, twisting and shearing) of the magnetic field (*e.g.*, Berger & Field, 1984; Berger, 1999). Though the magnetic helicity is a useful quantity for characterising magnetic geometry, its application to FTEs remains limited. For our work, we consider the twisting feature of FTE flux ropes, which to first order can be described by the sign of magnetic helicity, *i.e.*,  $H = \pm 1$ . Here,  $H = +1$  corresponds to a twist in a right-handed (RH) sense, while  $H = -1$  corresponds to a twist in a left-handed (LH) sense. Some early works that study the magnetic helicity of magnetic flux ropes include Dasso et al. (2003), who studied the twist distribution of magnetic clouds in the solar wind, and Bothmer and Schwenn (1998), who studied the helicity sign of magnetic clouds and its association with the polarity of solar filaments on the Sun’s surface. More recently, Kieokaew et al. (2021) studied the helicity sign of FTEs and its relationship with the Interplanetary Magnetic Field (IMF). We follow an approach similar to Kieokaew et al. (2021).

Based on geometrical considerations for FTE formation under southward IMF conditions, Kieokaew et al. (2021) hypothesised that the flux rope twist direction should correspond to the IMF  $B_y$  orientation. This hypothesis arose from the configuration of magnetic reconnection in which the IMF  $B_y$  component would give a guide field to the reconnecting magnetic field between the draped, southward IMF and the northward geomagnetic field (Lee & Fu, 1985). In the context of FTE generation by multiple X-line reconnection, this guide field (IMF  $B_y$ ) orientation would directly determine the core field and the helicity sign of the flux rope formed between the two X-lines. Under southward IMF, an FTE formed in between multiple X-line reconnection would have a positive helicity sign if it is formed under IMF  $B_y > 0$  (*i.e.*, duskward), while it would have a negative helicity sign if it is formed under IMF  $B_y < 0$  (*i.e.*, dawnward). Using data from the Magnetospheric MultiScale (MMS) mission, they performed a statistical study of the helicity sign of FTE flux ropes. They found that the majority of events are consistent with this hypothesis. However, there were a significant number of events (14 out of 84) that were not consistent with this hypothesis. In other words, in some events, a duskward IMF  $B_y$  imposed both a duskward core field and a positive helicity, and in others, a dawnward IMF  $B_y$  imposed both a dawnward core field and a negative helicity. We adapt Figure 1 of Kieokaew et al. (2021) to illustrate the connection between the core field orientation and the helicity sign. Figure 1 shows a schematic illustration of a dawnward and southward IMF leading to a dawnward core field and left-handed flux rope. A duskward and southward IMF would have led to a duskward core field and a right-handed flux rope,

123 highlighting the one-to-one relationship between the core field orientation and the he-  
 124 licity sign that results from guide field reconnection in a scenario where the flux rope is  
 125 formed by multiple X-lines. In another study, Karimabadi et al. (1999) discussed, based  
 126 on 2-D and 3-D hybrid simulations, how the core field of flux ropes on the dayside mag-  
 127 netopause and the magnetotail are controlled by the guide field. Teh, Abdullah, and Hasbi  
 128 (2014) studied the core field of two flux ropes observed at the magnetopause under high  
 129 magnetic shear. They found that the polarity of the core field of one of the flux ropes  
 130 is opposite to the guide field produced by reconnection as observed near the flux ropes.  
 131 In this work, we expand the statistics of Kieokaew et al. (2021) by including FTE ob-  
 132 servations from the Cluster mission. We investigate in particular the FTE population  
 133 whose helicity sign is inconsistent with the IMF  $B_y$  orientation to understand their for-  
 134 mation mechanism.

135 The outline of this paper is as follows. Section 2 presents data from the Cluster and  
 136 MMS missions and the methodology for event selection and flux rope fitting. Section 3  
 137 presents an example event from MMS and the statistical analyses of all events. Section  
 138 4 discusses our findings. Finally, Section 5 presents the conclusions and summary.

## 139 2 Data and methodology

### 140 2.1 Data overview

141 We utilize data from the Cluster (Escoubet et al., 2001) and MMS (Burch et al.,  
 142 2016) missions. Cluster made observations at high latitudes ( $|Z_{GSE}| > 5 R_E$ ), while  
 143 MMS made observations at low latitudes ( $-5 R_E < Z_{GSE} < 5 R_E$ ). We take data  
 144 from Cluster 1 and Cluster 3. For MMS, we take data only from MMS 1 since all the  
 145 MMS spacecraft observe identical features across FTE scale size.

146 For Cluster, We use the FTE list from Fear et al. (2012). The observations were  
 147 made between November 2002 and June 2003 during the Cluster dayside season. We per-  
 148 formed a visual inspection to determine the FTE time interval for each event. The cri-  
 149 teria for selection are: (*i*) clear symmetric and bipolar variation of  $B_N$  (the magnetic field  
 150 component perpendicular to the unperturbed magnetopause), and (*ii*) a clear enhance-  
 151 ment in the magnetic field strength. For events observed using MMS, we obtained the  
 152 list of quasi force-free FTEs from Kieokaew et al. (2021). This list is a subset of the FTE

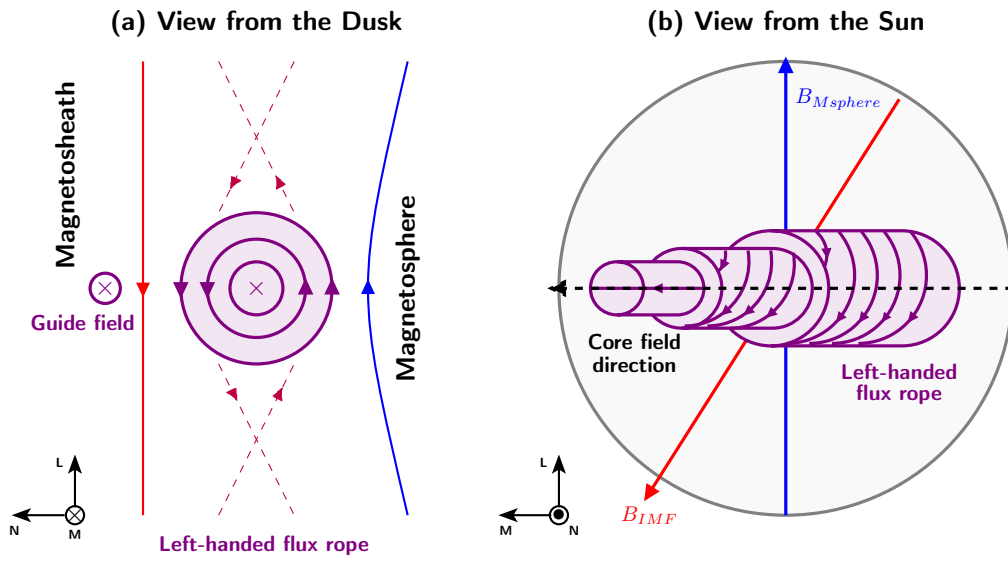


**Figure 1.** Schematic illustration of FTE formation by multiple X-line reconnection under a significant guide field. This illustration shows a dawnward and southward IMF leading to a dawnward core field and left-handed flux rope. Panel (a) shows a view from the dusk side and panel (b) shows a view from the sun. The FTE flux rope is represented in purple with arrows indicating the magnetic field direction. Solid blue and red lines represent magnetospheric and magnetosheath field lines, respectively. Adapted from Kieokaew et al. (2021).

153 observations using MMS in 2015 to 2017 (Phases A and B) compiled by Fargette et al.  
 154 (2020)

155 We use magnetic field measurements from the Flux Gate Magnetometer (FGM; Balogh  
 156 et al., 2001) instrument on-board Cluster at 0.2 s resolution in the Geocentric Solar Eclip-  
 157 tic (GSE) coordinate system. Similarly for MMS, we use magnetic field measurements  
 158 from the FGM instrument on-board MMS (Russell et al., 2016) in both burst and sur-  
 159 vey modes with resolutions of 0.01 s and 0.06 s, respectively. We use plasma moments  
 160 consisting of ion bulk flow velocity, ion temperature, and ion number density from the  
 161 Cluster Ion Spectrometry Hot Ion Analyser (CIS-HIA; Rème et al., 1997) instrument at  
 162 about 4s resolution on-board Cluster, and the Fast Plasma Investigation (FPI; Pollock  
 163 et al., 2016) measurements in both burst and survey modes with resolutions of 0.03 s/0.15  
 164 s (electrons/ions) and 4.5 s, respectively. Finally, we use solar wind data from the OMNI  
 165 database (King & Papitashvili, 2005), where the measurements were taken by the Ad-  
 166 vanced Composition Explorer (ACE) and Wind spacecraft and time-shifted to the bow-  
 167 shock nose, at 5-min resolution.

## 168 2.2 FTE observation

169 FTEs in spacecraft time-series data often exhibit clear signatures in the boundary  
 170 normal coordinate system (LMN) (*e.g.*, Russell & Elphic, 1979). In the LMN system,  
 171  $\mathbf{N}$  is normal to the magnetopause and pointing outward from the Earth,  $\mathbf{M}$  the cross  
 172 product of  $\mathbf{N}$  and the north geomagnetic dipole  $Z_{GSM}$  direction ( $\mathbf{M} = \mathbf{N} \times \mathbf{Z}_{GSM}$ ),  
 173  $\mathbf{L}$  completes the right-handed orthonormal system. We adopt the magnetopause model  
 174 from Shue et al. (1998) for locating the normal direction of the unperturbed magnetopause  
 175 boundary. The Shue model describes the shape, size and location of the magnetopause  
 176 boundary based on the function  $r = r_0 \left( \frac{2}{1 + \cos \theta} \right)^{\alpha_{MP}}$ , where  $r_0$  is the stand-off distance  
 177 of the magnetopause from the Earth,  $\alpha_{MP}$  is the level of tail flaring,  $\theta$  is the angle be-  
 178 tween the  $r_0$  and  $r$  directions.  $r_0$  and  $\alpha_{MP}$  are empirical functions of the IMF  $B_z$  and  
 179 the solar wind dynamic pressure ( $P_{dyn}$ ), given as  $r_0 = [10.22 + 1.29 \times \tanh(0.184 \times (B_z + 8.14))] \times$   
 180  $P_{dyn}^{-1/6.6}$  and  $\alpha_{MP} = (0.58 - 0.007 \times B_z) \times (1 + 0.024 \times \ln(P_{dyn}))$ .

181

### 2.3 Flux rope fitting

182

183

184

185

186

187

188

189

190

191

To obtain the helicity sign of FTE flux ropes, we fit the data to a force-free model derived by Burlaga (1988), which was originally introduced to describe the magnetic field structure of magnetic clouds in the solar wind. The model is a solution of the cylindrically symmetric force-free configuration satisfying the equation  $\nabla \times \mathbf{B} = \alpha \mathbf{B}$ , where  $\mathbf{B}$  is the magnetic field and  $\alpha$  is a constant, found by Lundquist (1950). The solution is found to be:  $B_A = B_0 J_0(\alpha R)$  for the axial component,  $B_T = B_0 H J_1(\alpha R)$  for the tangential component and  $B_R = 0$  for the radial component, where  $H = \pm 1$  is the helicity sign,  $R$  is the radial distance from the axis,  $J_0$  and  $J_1$  are the zeroth and first order Bessel functions of first kind, respectively, and  $B_0$  is the maximum magnetic field strength inside the flux rope.

192

193

194

195

196

197

198

199

200

201

202

203

204

205

206

207

208

209

210

211

212

213

As introduced in Burlaga (1988), the model fitting is done in a local flux rope frame  $(\mathbf{x}_v, \mathbf{y}_v, \mathbf{z}_v)$  (see Figure S1 of Kieokaew et al. (2021), adapted from Figure 2 of Burlaga (1988)). We use a more adapted frame similar to that used in Lepping et al. (1990). We take  $\mathbf{x}_v$  to be along the direction opposite to the flux rope motion such that  $\mathbf{x}_v = -\mathbf{V}_{av}/|\mathbf{V}_{av}|$ , where  $\mathbf{V}_{av}$  is the average flow velocity across the flux rope. We define  $\mathbf{z}_v = \mathbf{n}$ , where  $\mathbf{n}$  is the normal to the model magnetopause and  $\mathbf{y}_v$  completes the right-handed orthonormal system, *i.e.*,  $\mathbf{y}_v = \mathbf{z}_v \times \mathbf{x}_v$ . The five parameters describing the flux rope configuration in a local flux rope frame  $(\mathbf{x}_v, \mathbf{y}_v, \mathbf{z}_v)$  are: (i)  $\theta_0 \in [-90^\circ, 90^\circ]$  the angle between the flux rope axis and the ecliptic plane, (ii)  $\phi_0 \in [0^\circ, 180^\circ]$  the angle between the axial direction of the flux rope projected on the ecliptic plane and  $\mathbf{x}_v$ , (iii)  $b_0$  the distance between the spacecraft and the flux rope motion plane, (iv)  $t_0$  the time that corresponds to the closest approach of the flux rope to the spacecraft and (v)  $\alpha$  is a constant. The helicity sign  $H$  is determined from magnetic field data. Nevertheless, we confirm the helicity sign based on the quality of the resulting fit. As not all flux ropes can be assumed force-free, the quality of the fit is not always good. Here we select only flux ropes that can be fitted well to the model (*i.e.*, quasi force-free), and for which there is no ambiguity on the helicity sign. We selected 166 events in total that can be relatively well-described by the model, consisting of 82 events by Cluster (this list is a subset of Fear et al. (2012)'s initial list), added to the 84 events from MMS previously studied by Kieokaew et al. (2021). Table S1 of the supplementary information for this work lists the 82 events from Cluster with their respective start and end times, their locations in the GSE system and their helicity signs. The MMS events may be found in Table S1 of Kieokaew et al. (2021).

### 3 Event illustration & statistical analyses

#### 3.1 Event overview

Figure 2 shows an example of an FTE, detected by MMS1 on November 5<sup>th</sup>, 2015, between 14:07:07 and 14:07:44 UT. It shows a 10-min interval (top) and a zoom-in (1-min interval; bottom). Panels (a) and (a') present the magnetic field in the GSE coordinate system and its magnitude  $|\mathbf{B}|$ . Panel (b') present the components of the magnetic field in the  $(\mathbf{x}_v, \mathbf{y}_v, \mathbf{z}_v)$  frame. Panel (b) shows the components of the ion velocity in the GSE coordinate system. Panel (c) displays the ion number density. Panel (d) shows the ion temperature in the direction parallel and perpendicular to the magnetic field. Panel (e) presents the ion energy spectrogram. The bipolar signature of the flux rope is visible in panels (a) as shaded in gray, but it is most clearly seen in panel (b') where the  $B_{z_v}$  component rotates from negative to positive. We also observe an enhancement in the magnetic field strength in panel (a) and (a') during this bipolar variation. In addition, we also observe a slight increase in the temperature in panel (d) during the flux rope interval. The dashed lines in panel (b') represent the flux rope model fit during the flux rope time interval. In this case, the better fit was found for  $H = -1$ . Therefore, this flux rope twist is categorized as left-handed (LH). To understand the local conditions surrounding this flux rope, we also characterize the adjacent magnetospheric and magnetosheath regions as follows. The region highlighted in red in panels (a) to (e) shows the magnetosphere region adjacent to the flux rope, which is marked between 14:13:45 and 14:14:00 UT. This region is identified by an almost instantaneous drop in the ion number density seen in panel (c) co-located with a dropout in the fluxes of low energy ( $< 1$  keV) ions, and with intense fluxes of higher energy ions ( $> 1$  keV) that is distinct from the surrounding regions. The region highlighted in green shows the magnetosheath region most adjacent to the flux rope, between 14:06:40 and 14:06:55 UT. This region is identified with the larger density and lower temperature.

#### 3.2 Spatial distribution

Figure 3 shows the spatial distribution of all the events in the GSE coordinate system. Crosses represent RH ( $H = +1$ ) flux ropes and triangles represents LH ( $H = -1$ ) flux ropes. Panel (a) shows a projection in the  $Y_{GSE}-Z_{GSE}$  plane as viewed from the Sun (positive  $X_{GSE}$ ), and panel (b) is a projection in the  $X_{GSE}-Y_{GSE}$  plane as viewed

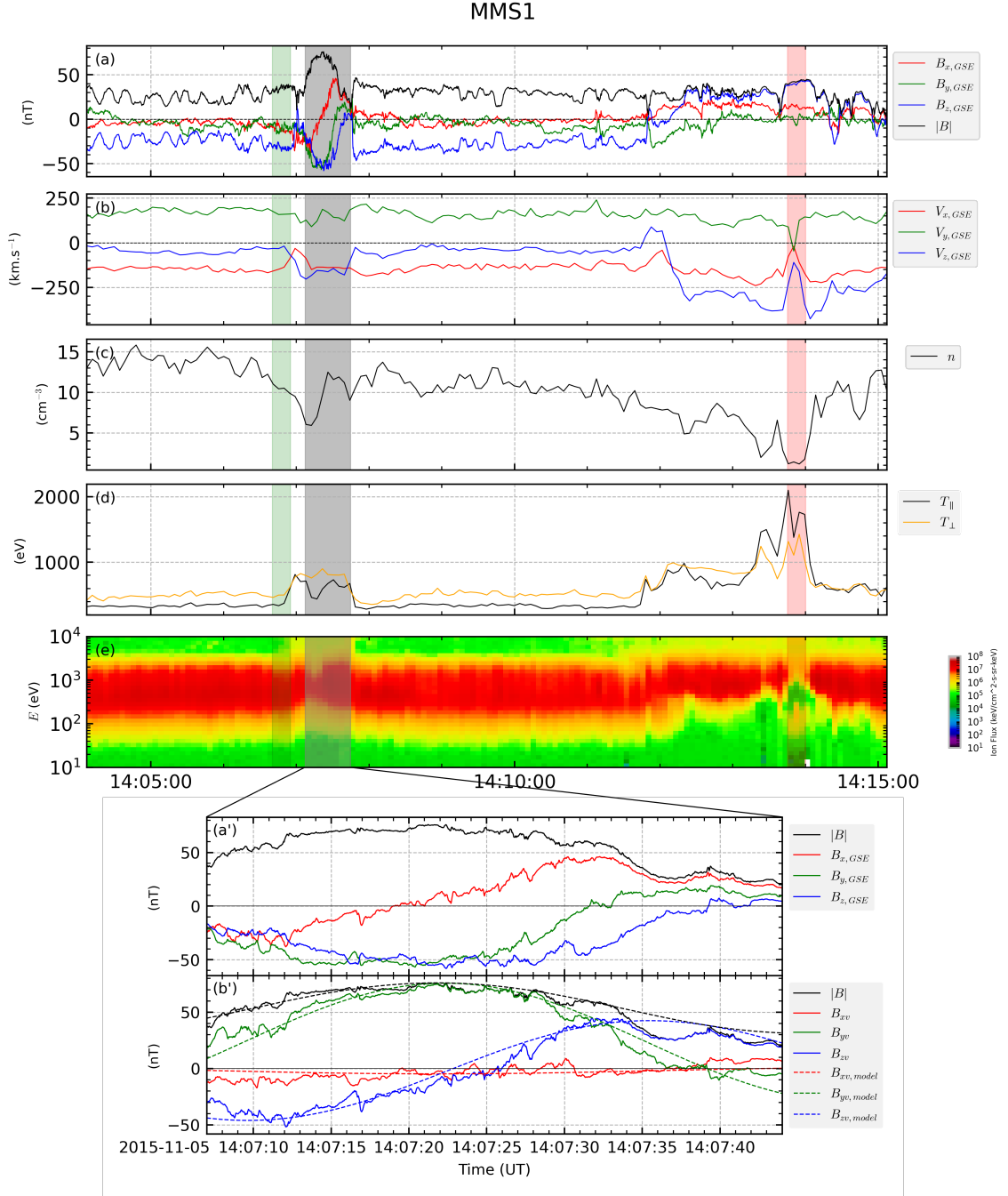


**Figure 2.** MMS observations of an FTE shown for a 10-min interval (top; panels (a) to (e)) and a 1-min interval (bottom; panels (a') and (b')). The FTE is highlighted in gray in the top panels. Panels (a) show the magnetic field in the GSE coordinate system. Panels (b), (c), (d) show the ion bulk velocity in the GSE coordinate system, the ion number density, and the ion temperature, respectively. Panel (e) shows the ion energy spectrogram. The green and red shaded regions mark the adjacent magnetosheath and magnetospheric regions to the FTE, respectively. Panels (a') and (b') show the zoom-in of the panels (a) in GSE and  $(x_v, y_v, z_v)$  coordinates system, respectively.

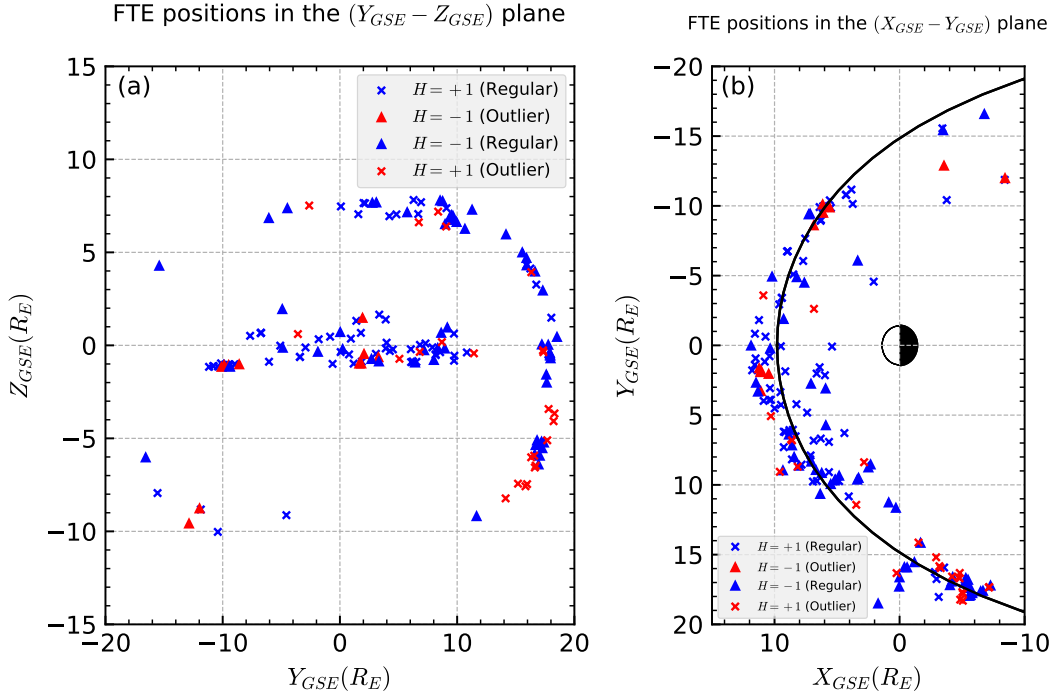


**Figure 3.** Spatial distribution of the FTEs in the GSE coordinate system in the (a) Y-Z and (b) X-Y planes. The RH ( $H = +1$ ) events are denoted by crosses and the LH ( $H = -1$ ) events are denoted by triangles. We distinguish the outlier events (in red) and regulars (in blue).

The solid black line in panel (b) represents the magnetopause boundary from the Shue model with  $r_0 = 9.8 R_E$  and  $\alpha_{MP} = 5.6$ .

245 from the north (positive  $Z_{GSE}$ ), with the approximate magnetopause boundary using  
 246 the average IMF  $B_z$  and  $P_{dyn}$  from the Shue model. The MMS events are located in the  
 247 low latitude region, while Cluster events are located at higher latitudes and further from  
 248 the nose. There are more events on the dusk side (positive  $Y_{GSE}$ ) than on the dawn side.  
 249 From our investigation, these events are often found downstream of quasi-perpendicular  
 250 shocks, where the magnetosheath data are often more laminar (which lead to an easier  
 251 identification of FTEs). Nevertheless, there is no spatial preferences for the RH and LH  
 252 flux ropes as they appear to be distributed almost uniformly across the planes.

### 253 3.3 Solar wind conditions

254 To revisit the correlation between the IMF  $B_y$  and the FTE helicity sign, we anal-  
 255 yse the IMF conditions preceding the detection of the FTEs, which would affect the lo-

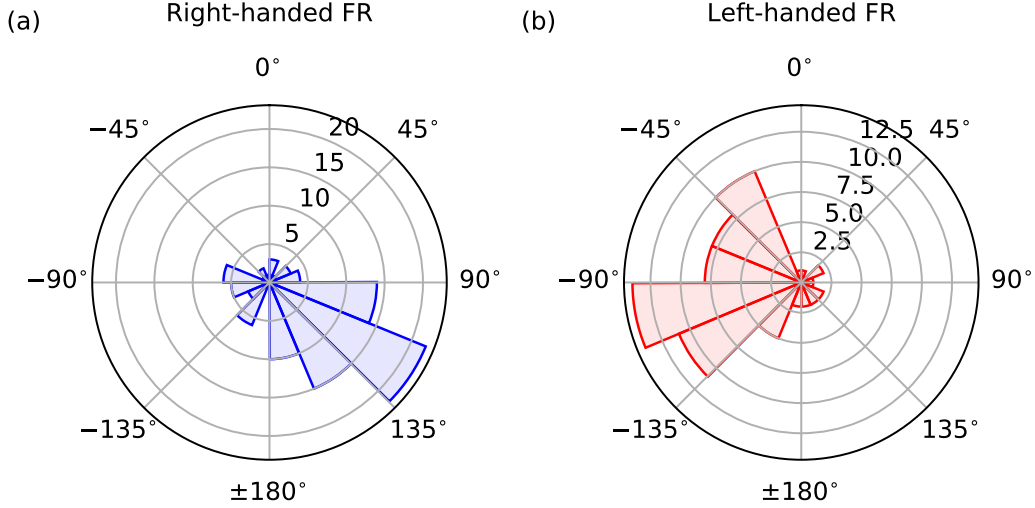
cal conditions in which magnetic reconnection takes place on the dayside magnetopause. As OMNI data provide solar wind conditions at the nose of the bowshock, we estimate the propagation time of the solar wind flow to be approximately 15 minutes to cross the magnetosheath and reach the magnetopause. The results are not sensitive with intervals between 15 and 30 minutes.

Figure 4 shows the distribution of the 15-min averaged IMF clock angles ( $\theta_{CA} = \arctan(B_y/B_z)$ ) preceding the events in polar histograms. Panel (a) shows the distribution for RH events and panel (b) shows the distribution for LH events. Positive IMF clock angles ( $0^\circ < \theta_{CA} < 180^\circ$ ) correspond to duskward IMF  $B_y$ , while the negative IMF clock angles ( $-180^\circ < \theta_{CA} < 0^\circ$ ) correspond to dawnward IMF  $B_y$ . Figure 4 shows that the majority of RH events are preceded by positive IMF clock angles (IMF  $B_y > 0$ ) as seen in panel (a), while the majority of the LH events are preceded by negative IMF clock angles (IMF  $B_y < 0$ ) as seen in panel (b). This group where the FTE helicity sign corresponds to the IMF  $B_y$  is referred as the regular group. This group is consistent with a flux rope generation by the multiple X-line reconnection scenario as explained in Kieokaew et al. (2021). However, in Figure 4, there are some events where the helicity sign does not correspond to the IMF  $B_y$  for both RH events and LH events. This group, in which we call the “outliers”, constitutes 21% of all events. We distinguish the spatial distribution of the outlier group with the red colour in Figure 3, while the regular group is presented in blue.

To investigate the solar wind conditions that might control the regular and outlier events, we also investigate other parameters such as the ion bulk velocity, ion number density, Mach number, and ion temperature. We do not find a correlation between those upstream parameters and the flux rope helicity sign. To investigate local effects, we investigate the conditions at the magnetopause where the FTEs may be generated. In particular, we focus on the local magnetic shear properties between the magnetosheath and the magnetospheric magnetic fields in the vicinity of the FTEs.

### 3.4 Local magnetic shear properties

As there is no clear correlation between the upstream solar wind parameters and the helicity sign of the outlier group, we now shift our focus to investigate local magnetopause properties. We employ two approaches to determine the local magnetic shear.



**Figure 4.** Distribution of the averaged IMF clock angle for (a) RH events, (b) LH events.

287 First, we explore the model developed by Trattner et al. (2007) that estimates the lo-  
 288 cal shear angle across the magnetopause surface by assuming a draping of the IMF and  
 289 the local flow (Cooling et al., 2001). For a given averaged IMF clock angle for each FTE,  
 290 we obtain a spatial distribution of the magnetic shear on the magnetopause surface. Fig-  
 291 ure 5 shows the local, 2-D magnetic shear angle map for a given IMF clock angle at  $225.5^\circ$   
 292 (IMF cone angle at  $99^\circ$  and dipole tilt angle at  $-8^\circ$ ) on the magnetopause in the  $(Y_{GSM}, Z_{GSM})$   
 293 plane on November 5, 2015, at 14:07:07 UT; the black cross (at  $Y = 5.5 R_E, Z = -3.4 R_E$ )  
 294 locates the position of the FTE. This approach allows us to model local magnetic shear  
 295 at the FTE location, which may indicate the local condition in which the FTE is formed,  
 296 *e.g.*, by magnetic reconnection near the location of the FTE. Figure 6 shows a histogram  
 297 of the distribution of the magnetic shear angle modelled at the FTE location for all 166  
 298 events. We categorize the data into the regular and outlier groups, represented by solid  
 299 black and dashed red lines, respectively. We find that the majority of the outlier group  
 300 has large magnetic shears with the events being mainly around  $150^\circ$ . In contrast, we find  
 301 that the regular flux ropes have a broader distribution centered around moderate mag-  
 302 netic shear angles. To check whether the magnetic shear angles from the model are con-  
 303 sistent with the observed shear properties, we also obtain local shear angles using the  
 304 data surrounding the outlier flux ropes. The procedure is as follows. We select two re-  
 305 gions, one in the magnetosphere and one in the magnetosheath. The magnetosphere has  
 306 low density but high temperature, while the magnetosheath has a larger density and lower

307 temperature. We avoid strong current layers, regions with jets, accelerated particles or  
 308 other flux ropes, throughout the selection process. We find that most of the flux ropes  
 309 are found on the magnetosheath side in the observations. We select a magnetosheath re-  
 310 gion and a magnetosphere region that are adjacent or close to the studied flux rope. The  
 311 magnetosphere is generally found from 1-min to 1-hour away from the flux rope (Fig-  
 312 ure 2). We calculate the shear angle by calculating  $\arccos\left(\frac{\mathbf{B}_{sp} \cdot \mathbf{B}_{sh}}{|\mathbf{B}_{sp}| |\mathbf{B}_{sh}|}\right)$ , where  $\mathbf{B}_{sp}$  is the  
 313 magnetic field vector in the magnetosphere, and  $\mathbf{B}_{sh}$  is the magnetic field vector in the  
 314 magnetosheath. The results are also shown in Figure 6 as denoted by the dashed blue  
 315 line. The magnetic shear angles obtained from this alternative method are consistent with  
 316 the results from the modeling.

## 317 4 Discussion

318 We have investigated the helicity sign of 166 quasi force-free FTEs, with 82 from  
 319 Cluster and 84 from MMS observations. We found that the helicity sign of most events  
 320 is ordered by the IMF  $B_y$  polarity, and so that positive IMF clock angles correspond to  
 321 duskward IMF  $B_y$ , while negative IMF clock angles ( $180^\circ < \theta_{CA} < 0^\circ$ ) correspond  
 322 to dawnward IMF  $B_y$ . We also found that 21% of the events have a helicity sign that  
 323 does not correspond to the expected IMF  $B_y$  polarity. Our findings are consistent with  
 324 the main results of Kieokaew et al. (2021) (right-handed FTEs are associated with posi-  
 325 tive IMF  $B_y$  and left-handed FTEs are associated with negative IMF  $B_y$ ). To investi-  
 326 gate the local conditions associated with the FTE formation, we have analysed the mag-  
 327 netic shear angle using both modelling and in-situ data at the FTE locations. We found  
 328 that the majority of the outlier FTEs (those whose helicity does not correspond to the  
 329 expected IMF  $B_y$ ) are located in generally higher magnetic shear regions.

330 As a first simple explanation, for a given small IMF  $B_y$  the determination of the  
 331 core field and helicity sign at low guide field (e.g., for high shears) may be more random  
 332 because of the uncertainties in mapping the IMF observations to the magnetopause (mak-  
 333 ing the helicity - IMF  $B_y$  relation less clear at low guide field). Karimabadi et al. (1999)  
 334 showed, based on simulations, that the Hall magnetic field plays a key role in determin-  
 335 ing the core field of flux ropes. We here utilize this conclusion to explain our results. In  
 336 other words we propose that the helicity and core field of outlier FTEs may be explained  
 337 by the combination of the Hall and guide fields (e.g., Aunai et al., 2011), during low guide  
 338 field conditions, rather than just randomness, as explained next.

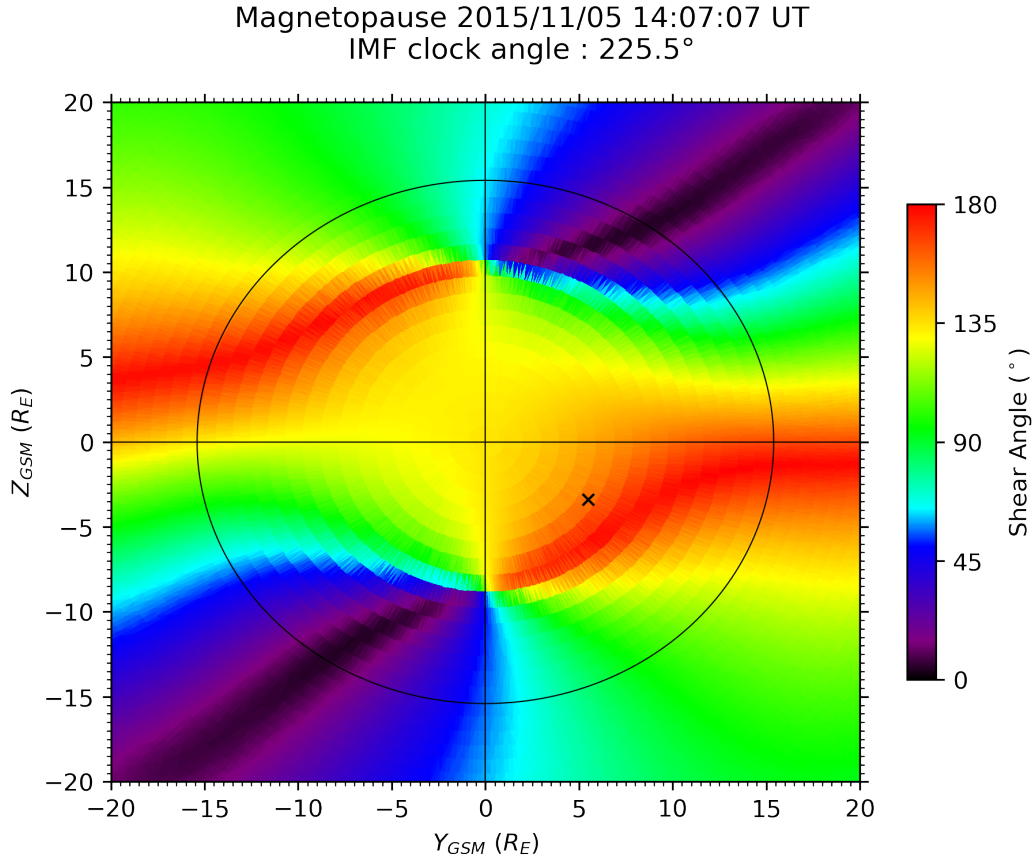


**Figure 5.** The magnetic shear angle map at the magnetopause surface projected onto the  $Y$ - $Z$  plane of the GSM coordinate system. The map is obtained for the event in Figure 1 on November 5<sup>th</sup>, 2015 at 14:07:07 UT produced using the averaged IMF clock angle (at 225.5°) preceding the event. The color scale represents the local magnetic shear angle from 0° (dark purple; no shear) to 180° (red; highest shear). The black cross marks the FTE location. The black circle denotes the terminator ( $X_{GSM} = 0$ ).

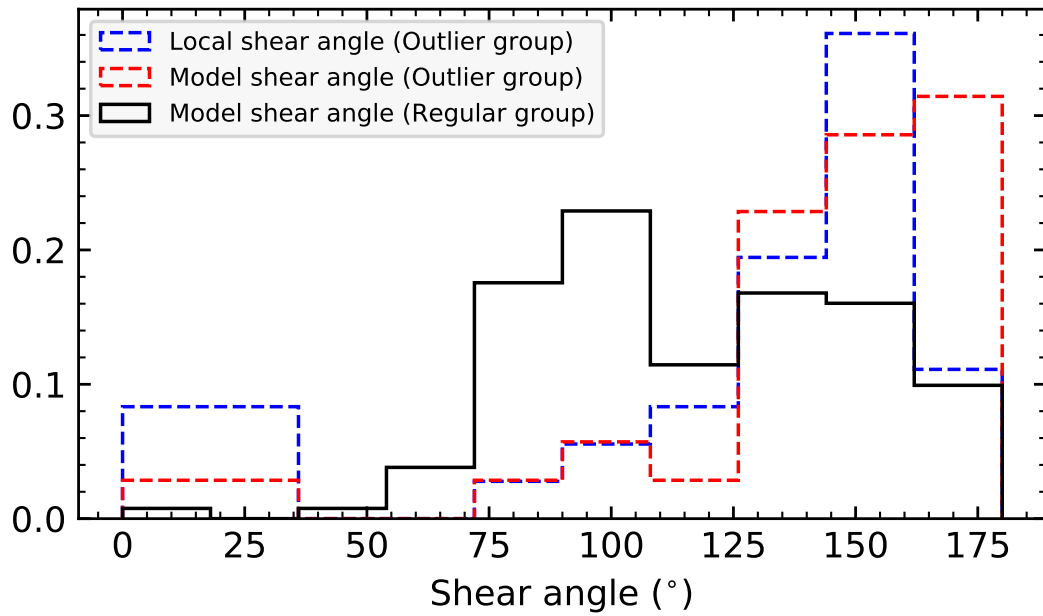


**Figure 6.** Distributions of the magnetic shear angle associated with the FTEs. The distributions of regular and outlier groups obtained from the model (Trattner et al. (2007)) are shown with black solid and red dashed lines, respectively. The distribution of the outlier group obtained from in-situ data is shown in blue dashed line. The distributions are normalized to the total number of each group.

339 Our findings in Figure 6 show that the outlier flux ropes (shown in red and in blue)  
 340 are mostly characterised by high magnetic shears, while the regular flux ropes (shown  
 341 in black) show a broader distribution centered on more moderate magnetic shear. This  
 342 finding suggests that the core field and helicity sign of flux ropes is affected by the lo-  
 343 cal magnetic shear properties in their vicinity. Assuming the magnetic shear at the FTE  
 344 generation site is not too different from that at their observed locations, we may con-  
 345 sider a core field and thus helicity generation mechanism as explained next. In the pres-  
 346 ence of a significant guide field, e.g., at moderate shear angle, the core field and the he-  
 347 licity sign of the generated FTE are likely determined by the guide field of magnetic re-  
 348 connection *e.g.*, Karimabadi et al. (1999). Since the IMF  $B_y$  is the main component that  
 349 provides the reconnection guide field under southward IMF conditions, the helicity sign  
 350 of the produced FTE therefore corresponds to the IMF  $B_y$  polarity. This mechanism may  
 351 explain the regular flux ropes found in our study and in Kieokaew et al. (2021). In the  
 352 presence of a weak guide field, e.g., at higher magnetic shear, however, the determina-  
 353 tion of the FTE core field and helicity appears less clear. We explain below that the Hall  
 354 physics of magnetic reconnection in the absence of guide field may determine these prop-  
 355 erties, Karimabadi et al. (1999).

356 Near the X-line of anti-parallel magnetic reconnection, *i.e.*, in the ion diffusion re-  
 357 gion, the Hall electric field is produced as ions meander around the magnetic null while  
 358 electrons remain frozen-in. Under symmetric inflow conditions, this Hall electric field drags  
 359 out the newly reconnected magnetic fields and produces a quadrupolar pattern in the  
 360 out-of-plane (guide field) direction (*e.g.*, Mandt et al., 1994; Nagai et al., 2001; Borg et  
 361 al., 2005; Denton et al., 2016). At the dayside magnetopause, magnetic reconnection is  
 362 asymmetric due to the denser plasma in the magnetosheath. Thus, the Hall field pat-  
 363 tern on the magnetosheath side dominates and leads to a more bipolar Hall pattern (*e.g.*,  
 364 Karimabadi et al., 1999; Eastwood et al., 2013; Zhang et al., 2017). Since the outlier events  
 365 are mostly found for high magnetic shears, we expect that their core field, and in turn  
 366 their helicity, is determined by the Hall field, consistent with previous works by Karimabadi  
 367 et al. (1999), Teh, Abdullah, and Hasbi (2014) and Teh, Nakamura, et al. (2014).

368 To summarize the process explained above, Figure 7 shows a schematic of FTE flux  
 369 rope generation in asymmetric magnetic reconnection under magnetopause-like condi-  
 370 tions. Panel (a) shows conditions without a guide field, *i.e.*, anti-parallel reconnection,  
 371 while panel (b) shows the conditions with a guide field, *i.e.*, component reconnection.

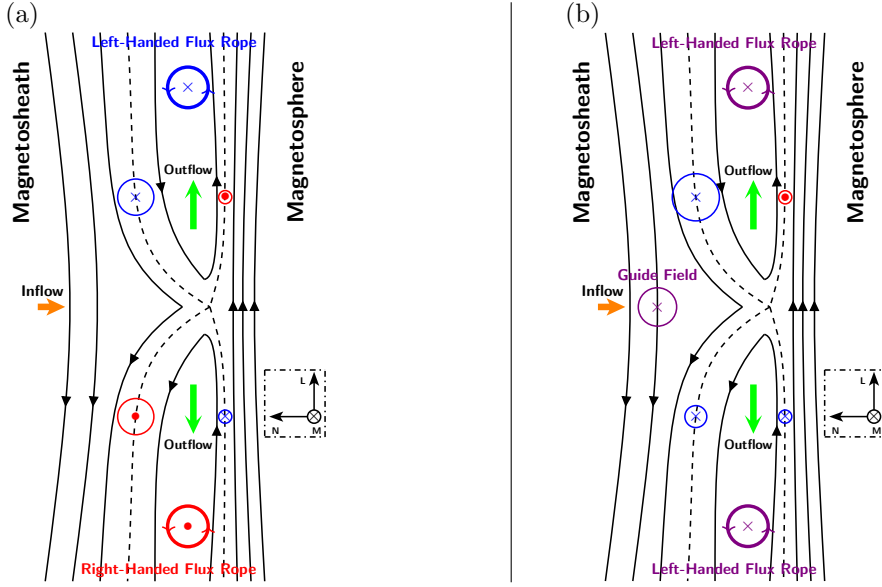


**Figure 7.** Schematic illustration of (a) anti-parallel and (b) component or guide field magnetic reconnection. Solid black lines represent the magnetic field lines and the dashed black lines represent the separatrices. Blue and red circles represent the Hall pattern, with their sizes corresponding to the magnitude of the Hall field which is stronger in the magnetosheath side due to the asymmetry in the inflow plasma density. In panel (b), the purple circle represents the guide field. The thicker circles represent the flux ropes generated in the reconnection exhausts. Green arrows represent the reconnection outflow, while orange arrows represent the inflow.

372 The solid black lines denote the projection of magnetic field lines and the dashed black  
 373 lines denote the separatrices, with black arrows heads indicating their directions. We mark  
 374 the plasma inflow with an orange arrow and the plasma outflows with green arrows. The  
 375 Hall pattern is represented by the circles with crosses or dots on the separatrices indi-  
 376 cating the in- and out- of-plane magnetic field directions, respectively. In panel (a), the  
 377 guide field is absent (or weak), and the Hall magnetic field pattern is more dominant on  
 378 the magnetosheath side than the magnetospheric side due to the denser plasma (Mozer  
 379 & Hull, 2010); we denote this dominant Hall field with the bigger circles. In this case,  
 380 the Hall pattern on the magnetosheath side determines the core field of the flux ropes,  
 381 and in turn the helicity; they are represented by the thick blue and red circles. In panel  
 382 (b), however, the presence of a significant guide field reverses the effect of the out of plane  
 383 Hall field and/or to first order adds up with it to determine the core field and helicity  
 384 of the FTEs. They are illustrated with purple circles, *e.g.*, for inward guide field. In brief,

385 these scenarios explain how the FTEs generate their core fields under anti-parallel (high  
 386 shear) and component (moderate shear) magnetic reconnection (Karimabadi et al., 1999),  
 387 leading to helicity signs as reported in our study. This scenario is confirmed with sim-  
 388 ulation results in the next paragraph.

389 The present study corroborates previous work on FTE core field generation as a  
 390 result of the Hall pattern. While to our knowledge our study is the first to present in-  
 391 situ observations of this process, previous simulations by Karimabadi et al. (1999) found  
 392 such pattern. Figure 8 shows simulation results from the magnetohydrodynamic with  
 393 embedded particle-in-cell (MHD-EPIC) model. It shows the magnetic field  $B_y$  compo-  
 394 nent in the  $X - Z$  plane of the GSM system, *i.e.*, as viewed from the dawn side. The  
 395 simulation has been published in Chen et al. (2020). Panels (a) and (b) show the time  
 396 evolution of FTE generation due to sequential reconnection X-line under purely south-  
 397 ward IMF conditions. The box delineated by a black line represents the region that is  
 398 simulated using the PIC code to include the kinetic physics of magnetic reconnection.  
 399 Here, panel (a) shows the first reconnection X-line formation as marked by a red star.  
 400 The polarity of  $B_y$  north and south of the X-line shows negative and positive values, re-  
 401 spectively. This bipolar  $B_y$  variation is the bipolar Hall pattern produced as a consequence  
 402 of asymmetric reconnection with the denser plasma in the magnetosheath side. Panel  
 403 (b) shows the simulation about 7 minutes later when the first X-line has propagated north-  
 404 ward while the second and the third reconnection X-lines sequentially appear as marked  
 405 with gray stars. Between the first and second X-lines in panel (b), as zoomed-in in panel  
 406 (c), an FTE bounded by a white contour forms. The key observation here is that the core  
 407 field of this FTE retains the Hall pattern of the two X-lines. In other words, panel (c)  
 408 illustrates an example of how an FTE generates its core field from the Hall magnetic field  
 409 of magnetic reconnection. Additionally, panel (d) shows a zoom-in of the second and third  
 410 X-lines. Here, another FTE with the same core field as generated by the initial Hall per-  
 411 turbation is also being formed. Despite the Hall magnetic field perturbation, the forma-  
 412 tion of the FTEs follows the standard mechanism proposed by Raeder (2006) under large  
 413 dipole tilt angle, where an FTE can be generated between multiple X-lines. Based on  
 414 our statistical results and this simulation work, we conclude that the outlier FTEs core  
 415 fields and ensuing helicity are determined from the Hall magnetic field of magnetic re-  
 416 connection for a weak guide field condition. In brief, the Hall magnetic reconnection leads  
 417 to the core field and thus the helicity sign of FTEs in the absence of a guide field.

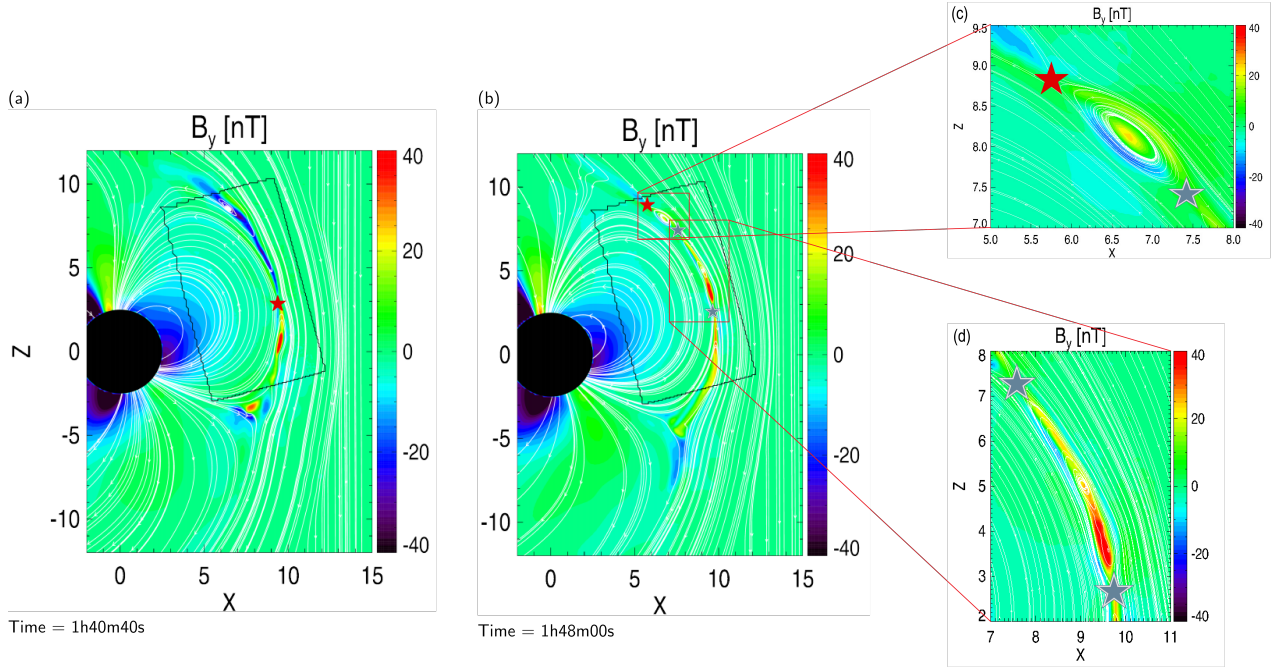


**Figure 8.** The evolution of the dayside magnetopause using a global MHD simulation embedded with PIC code for the area delineated by a black square. The simulation shows the magnetic field  $B_y$  component in the  $X - Z$  plane in the GSM coordinate system as viewed from the dawn side. Panel (a) shows a snapshot where a reconnection X-line is first formed as marked by a red star. Panel (b) shows a snapshot around 7 minutes later of panel (a) where the second and third X-lines, marked by gray stars, are now formed. Panel (c) shows a zoom-in of an FTE formation between the first and the second X-lines. Panel (d) shows a zoom-in of another FTE formation between the second and the third X-lines.

418 The generation of FTEs by multiple X-lines is not just an assumption in our study  
 419 (see Figure 1 and Section 1) as it is in fact the only valid paradigm to interpret our re-  
 420 sults. Indeed, considering the role of the Hall magnetic field in determining both the core  
 421 field and helicity sign flux ropes suggests that the single X-line mechanism, under low  
 422 guide field, would always create a left-handed flux rope northward of the reconnection  
 423 site and a right-handed flux rope southward of the reconnection site, as shown in Fig-  
 424 ure 7a. If it were the case, this would lead to a systematic north-south dichotomy in left-  
 425 handed and right-handed flux ropes for the outlier group (which occur for low guide field),  
 426 while this is not observed in-situ. In particular this trend is not observed in Figure 3 where  
 427 the red crosses and triangles denote the outlier flux ropes (respectively right- and left-

428 handed). Our findings thus support the idea that FTE flux ropes are produced through  
 429 a multiple X-line mechanism.

430 So far our discussion on the role of the Hall magnetic field in determining the core  
 431 field neglected the fact that we are adopting multiple X-line reconnection as a forma-  
 432 tion mechanism of FTEs. There should be two distinct Hall patterns that would be present  
 433 at the two X-lines surrounding the FTE flux rope, and that may affect the internal mag-  
 434 netic structure of the FTE. In other words, the Hall pattern is present in the exhausts  
 435 of the two X-lines surrounding the FTE flux rope. In a low guide field scenario, one of  
 436 the two Hall signatures may determine the core field of the FTE flux rope. But this raises  
 437 the question of which X-line is dominant or which X-line controls the core field and he-  
 438 licity sign of the flux rope. Different parameters could come into play to determine which  
 439 X-line Hall field become dominant. In particular, the simulations of Figure 8 suggest that  
 440 the initial X-line Hall pattern may be dominant. Thus the temporal sequence of X-line  
 441 formation appears important in the determination of the flux rope core field and the he-  
 442 licity sign. So far, we have conducted only one such simulation and additional simula-  
 443 tions would be required to confirm this first result. In particular, one may expect that,  
 444 in addition to the temporal sequence, the reconnection rate at each X-line may have an  
 445 impact on which Hall field pattern may eventually dominate the flux ropes topology. We  
 446 also note that an FTE formation may be a continuous process where active magnetic re-  
 447 connection can continuously feed magnetic fluxes into the flux rope, resulting in the FTE  
 448 growth (*e.g.*, Akhavan-Tafti et al., 2019; Hoilijoki et al., 2019). The core field of an FTE  
 449 may thus be an accumulative effect of multiple reconnection with a varying reconnect-  
 450 tion rate depending on solar wind conditions. All these aspects deserved to be further  
 451 investigated but they are left for future work.

## 452 5 Summary and conclusions

453 We have statistically studied the helicity sign of 166 quasi force-free FTEs, 82 of  
 454 which were observed by Cluster, and 84 by MMS. We have found that the helicity sign  
 455 of the majority of the events corresponds to the IMF  $B_y$  polarity. We call this popula-  
 456 tion of FTEs the regular group. However, we also found that the helicity sign of a sig-  
 457 nificant number of events (21% of the total events) does not correspond to the IMF  $B_y$   
 458 polarity. We call this population the outlier group. We have investigated the local prop-  
 459 erties of the magnetopause surrounding the FTE locations. In particular, we modeled,

460 based on the model by Trattner et al. (2007), the local magnetic shear angle for each FTE.  
 461 We have found that the regular group show a spread distribution centered around mod-  
 462 erate shear angles. For moderate and low shear, the guide field expected at the recon-  
 463 nection sites forming FTEs would control the core field of FTE, and thus control the he-  
 464 licity sign. This situation is consistent with the fact that the IMF  $B_y$  controls the he-  
 465 licity sign of the regular group as the IMF  $B_y$  represents the main component that pro-  
 466 vides the reconnection guide field (Kieokaew et al., 2021). For the outlier group, in ad-  
 467 dition to the model we have investigated the shear angle using in-situ data surrounding  
 468 each outlier FTE, and we found that they occur at higher magnetic shear locations mean-  
 469 ing lower guide field closer to anti-parallel magnetic reconnection regions. In this case,  
 470 it is less clear what controls the core field of the outlier FTEs. In particular, there are  
 471 higher uncertainties on the IMF mapping and therefore a higher randomness may be ex-  
 472 pected in the determination of helicity and core field under low guide field at the recon-  
 473 nection site. However, under such conditions another physical process may be at work  
 474 to determine the core field and helicity of flux ropes at the magnetopause. We displayed  
 475 simulations that show how the Hall effect in the reconnection site may control the core  
 476 field and helicity of FTEs. This effect of the Hall field on the core field of plasmoids was  
 477 initially proposed by Karimabadi et al. (1999) using 2-D and 3-D hybrid simulations with  
 478 no guide field.

479 At the magnetopause, anti-parallel magnetic reconnection is typically triggered un-  
 480 der asymmetric plasma conditions. In this case the Hall magnetic field has a strongly  
 481 skewed quadrupolar pattern, so that the pattern looks mostly bipolar with the Hall field  
 482 in the two exhausts having opposite out-of-plane orientations (Figure 7). This bipolar  
 483 Hall pattern in turn controls the core field of FTE flux ropes, and thus, controls their  
 484 helicity sign. The effect was shown using the results from a global MHD simulation with  
 485 embedded PIC code in Figure 8. Our study also supports the multiple X-line mechanism  
 486 for the process to produce FTEs as we do not observe any north-south dichotomy for  
 487 the right-handed and left-handed flux ropes for the outlier group, which occurs for low  
 488 guide field, while under such conditions a generation mechanism based on a single X-line  
 489 would suggest such a dichotomy between hemispheres. The presence of two X-lines in  
 490 the vicinity of FTE flux ropes means the existence of two distinct Hall patterns from the  
 491 two X-lines surrounding the FTE, but only one of them should dominate and determine  
 492 the core field and helicity of FTEs. For instance, in the case of Figure 8 we find that the

493 initial X-line is dominant and thus the temporal sequence of X-line formation appears  
 494 to play an important role in determining the dominant Hall effect on subsequent FTE  
 495 formation. Future work should look into this temporal sequence of X-line formation, and  
 496 its contribution in determining the dominant Hall field. Of course, attention should also  
 497 be given to the reconnection rate which should also come into play, in addition to the  
 498 temporal sequence. This work highlights an important aspect of the fundamental inter-  
 499 connection between kinetic scale processes of magnetic reconnection and the macroscale  
 500 structures of FTEs.

### 501 **Data availability information**

502 MMS, Cluster and OMNI data are available online at [https://lasp.colorado.edu/](https://lasp.colorado.edu/mms/sdc/public/)  
 503 [mms/sdc/public/](https://lasp.colorado.edu/mms/sdc/public/), <https://csa.esac.esa.int/csa-web/> and [https://omniweb.gsfc](https://omniweb.gsfc.nasa.gov/)  
 504 [.nasa.gov/](https://omniweb.gsfc.nasa.gov/), respectively.

### 505 **Acknowledgments**

506 Work at IRAP was supported by CNRS, CNES and UPS. Our analysis made use of the  
 507 tools developed at IRAP by the CDPP (AMDA <http://amda.cdpp.eu/>, and speasy  
 508 <https://pypi.org/project/speasy/> ) and by E. Penou (CL, [http://clweb.irap.omp](http://clweb.irap.omp.eu/)  
 509 [.eu/](http://clweb.irap.omp.eu/)). CDPP, the Centre de Données de la Physique des Plasmas, is supported by CNRS,  
 510 CNES, Observatoire de Paris and Université Paul Sabatier, Toulouse. R. C. Fear received  
 511 funding from Science and Technology Facilities Council Consolidated Grant ST/ V000942/1.

### 512 **References**

- 513 Akhavan-Tafti, M., Slavin, J. A., Sun, W. J., Le, G., & Gershman, D. J. (2019).  
 514 MMS Observations of Plasma Heating Associated With FTE Growth. *Geo-*  
 515 *physical Research Letters*, *46*(22), 12654–12664. doi: 10.1029/2019GL084843
- 516 Aunai, N., Retinò, A., Belmont, G., Smets, R., Lavraud, B., & Vaivads, A. (2011).  
 517 The proton pressure tensor as a new proxy of the proton decoupling region in  
 518 collisionless magnetic reconnection. *Annales Geophysicae*, *29*(9), 1571–1579.  
 519 Retrieved from <https://angeo.copernicus.org/articles/29/1571/2011/>  
 520 doi: 10.5194/angeo-29-1571-2011
- 521 Balogh, A., Carr, C. M., Acuña, M. H., Dunlop, M. W., Beek, T. J., Brown, P.,  
 522 ... Schwingenschuh, K. (2001). The Cluster Magnetic Field Investigation:

- 523 overview of in-flight performance and initial results. *Annales Geophysicae*,  
524 *19*(10/12), 1207-1217.
- 525 Berger, M. A. (1999, dec). Introduction to magnetic helicity. *Plasma Physics and*  
526 *Controlled Fusion*, *41*(12B), B167–B175. Retrieved from [https://doi.org/10](https://doi.org/10.1088/0741-3335/41/12b/312)  
527 [.1088/0741-3335/41/12b/312](https://doi.org/10.1088/0741-3335/41/12b/312) doi: 10.1088/0741-3335/41/12b/312
- 528 Berger, M. A., & Field, G. B. (1984). The topological properties of mag-  
529 netic helicity. *Journal of Fluid Mechanics*, *147*, 133–148. doi: 10.1017/  
530 S0022112084002019
- 531 Borg, A. L., Øieroset, M., Phan, T. D., Mozer, F. S., Pedersen, A., Mouikis,  
532 C., . . . Rème, H. (2005). Cluster encounter of a magnetic reconnect-  
533 tion diffusion region in the near-earth magnetotail on september 19,  
534 2003. *Geophysical Research Letters*, *32*(19). Retrieved from [https://](https://agupubs.onlinelibrary.wiley.com/doi/abs/10.1029/2005GL023794)  
535 [agupubs.onlinelibrary.wiley.com/doi/abs/10.1029/2005GL023794](https://agupubs.onlinelibrary.wiley.com/doi/abs/10.1029/2005GL023794) doi:  
536 <https://doi.org/10.1029/2005GL023794>
- 537 Bothmer, V., & Schwenn, R. (1998). The structure and origin of magnetic clouds  
538 in the solar wind. *Annales Geophysicae*, *16*(1), 1–24. doi: [https://doi.org/10](https://doi.org/10.1007/s00585-997-0001-x)  
539 [.1007/s00585-997-0001-x](https://doi.org/10.1007/s00585-997-0001-x)
- 540 Burch, J. L., Moore, T. E., Torbert, R. B., & Giles, B. L. (2016). Magnetospheric  
541 Multiscale Overview and Science Objectives. *Space Science Reviews*, *199*,  
542 5–21. doi: <https://doi.org/10.1007/s11214-015-0164-9>
- 543 Burlaga, L. F. (1988). Magnetic clouds and force-free fields with constant alpha.  
544 *Journal of Geophysical Research: Space Physics*, *93*(A7), 7217-7224. doi:  
545 <https://doi.org/10.1029/JA093iA07p07217>
- 546 Chen, Y., Tóth, G., Hietala, H., Vines, S. K., Zou, Y., Nishimura, Y., . . . Markidis,  
547 S. (2020). Magnetohydrodynamic with embedded particle-in-cell sim-  
548 ulation of the geospace environment modeling dayside kinetic processes  
549 challenge event. *Earth and Space Science*, *7*(11), e2020EA001331. Re-  
550 trieved from [https://agupubs.onlinelibrary.wiley.com/doi/abs/](https://agupubs.onlinelibrary.wiley.com/doi/abs/10.1029/2020EA001331)  
551 [10.1029/2020EA001331](https://doi.org/10.1029/2020EA001331) (e2020EA001331 10.1029/2020EA001331) doi:  
552 <https://doi.org/10.1029/2020EA001331>
- 553 Cooling, B. M. A., Owen, C. J., & Schwartz, S. J. (2001). Role of the magne-  
554 tosheath flow in determining the motion of open flux tubes. *Journal of*  
555 *Geophysical Research: Space Physics*, *106*(A9), 18763-18775. Retrieved

- 556 from <https://agupubs.onlinelibrary.wiley.com/doi/abs/10.1029/>  
 557 2000JA000455 doi: <https://doi.org/10.1029/2000JA000455>
- 558 Cowley, S. W. H. (1982). The causes of convection in the earth's magnetosphere:  
 559 A review of developments during the ims. *Reviews of Geophysics*, 20(3), 531-  
 560 565. Retrieved from [https://agupubs.onlinelibrary.wiley.com/doi/abs/](https://agupubs.onlinelibrary.wiley.com/doi/abs/10.1029/RG020i003p00531)  
 561 10.1029/RG020i003p00531 doi: <https://doi.org/10.1029/RG020i003p00531>
- 562 Dasso, S., Mandrini, C. H., Démoulin, P., & Farrugia, C. J. (2003). Magnetic  
 563 helicity analysis of an interplanetary twisted flux tube. *Journal of Geo-*  
 564 *physical Research: Space Physics*, 108(A10). Retrieved from [https://](https://agupubs.onlinelibrary.wiley.com/doi/abs/10.1029/2003JA009942)  
 565 [agupubs.onlinelibrary.wiley.com/doi/abs/10.1029/2003JA009942](https://agupubs.onlinelibrary.wiley.com/doi/abs/10.1029/2003JA009942) doi:  
 566 <https://doi.org/10.1029/2003JA009942>
- 567 Denton, R. E., Sonnerup, B. U. , Hasegawa, H., Phan, T. D., Russell, C. T.,  
 568 Strangeway, R. J., ... Torbert, R. B. (2016). Reconnection guide field and  
 569 quadrupolar structure observed by mms on 16 october 2015 at 1307 ut. *Jour-*  
 570 *nal of Geophysical Research: Space Physics*, 121(10), 9880-9887. Retrieved  
 571 from [https://agupubs.onlinelibrary.wiley.com/doi/abs/10.1002/](https://agupubs.onlinelibrary.wiley.com/doi/abs/10.1002/2016JA023323)  
 572 2016JA023323 doi: <https://doi.org/10.1002/2016JA023323>
- 573 Dorelli, J. C., & Bhattacharjee, A. (2009). On the generation and topology of flux  
 574 transfer events. *Journal of Geophysical Research: Space Physics*, 114(A6).  
 575 Retrieved from [https://agupubs.onlinelibrary.wiley.com/doi/abs/](https://agupubs.onlinelibrary.wiley.com/doi/abs/10.1029/2008JA013410)  
 576 10.1029/2008JA013410 doi: <https://doi.org/10.1029/2008JA013410>
- 577 Eastwood, J. P., Phan, T. D., Øieroset, M., Shay, M. A., Malakit, K., Swisdak,  
 578 M., ... Masters, A. (2013, nov). Influence of asymmetries and guide  
 579 fields on the magnetic reconnection diffusion region in collisionless space  
 580 plasmas. *Plasma Physics and Controlled Fusion*, 55(12), 124001. Re-  
 581 trieved from <https://doi.org/10.1088/0741-3335/55/12/124001> doi:  
 582 10.1088/0741-3335/55/12/124001
- 583 Escoubet, C. P., Fehringer, M., & Goldstein, M. (2001). Introduction the cluster  
 584 mission. *Annales Geophysicae*, 19(10/12), 1197-1200. doi: [https://doi.org/10](https://doi.org/10.5194/angeo-19-1197-2001)  
 585 .5194/angeo-19-1197-2001
- 586 Fargette, N., Lavraud, B., Øieroset, M., Phan, T. D., Toledo-Redondo, S., Kieokaew,  
 587 R., ... Smith, S. E. (2020). On the ubiquity of magnetic reconnection inside  
 588 flux transfer event-like structures at the earth's magnetopause. *Geophysical*

- 589 *Research Letters*, 47(6), e2019GL086726. (e2019GL086726 2019GL086726) doi:  
590 <https://doi.org/10.1029/2019GL086726>
- 591 Fear, R. C., Palmroth, M., & Milan, S. E. (2012). Seasonal and clock an-  
592 gle control of the location of flux transfer event signatures at the magne-  
593 topause. *Journal of Geophysical Research: Space Physics*, 117(A4). doi:  
594 <https://doi.org/10.1029/2011JA017235>
- 595 Hasegawa, H., Wang, J., Dunlop, M. W., Pu, Z. Y., Zhang, Q. H., Lavraud, B., ...  
596 Bogdanova, Y. V. (2010). Evidence for a flux transfer event generated by mul-  
597 tiple x-line reconnection at the magnetopause. *Geophysical Research Letters*,  
598 37, 1-6. doi: 10.1029/2010GL044219
- 599 Hoilijoki, S., Ganse, U., Sibeck, D. G., Cassak, P. A., Turc, L., Battarbee, M., ...  
600 Palmroth, M. (2019, jun). Properties of Magnetic Reconnection and FTEs on  
601 the Dayside Magnetopause With and Without Positive IMF B x Component  
602 During Southward IMF. *Journal of Geophysical Research: Space Physics*,  
603 124(6), 4037–4048. Retrieved from [https://onlinelibrary.wiley.com/doi/](https://onlinelibrary.wiley.com/doi/abs/10.1029/2019JA026821)  
604 [abs/10.1029/2019JA026821](https://onlinelibrary.wiley.com/doi/abs/10.1029/2019JA026821) doi: 10.1029/2019JA026821
- 605 Karimabadi, H., Krauss-Varban, D., Omidi, N., & Vu, H. X. (1999). Magnetic  
606 structure of the reconnection layer and core field generation in plasmoids.  
607 *Journal of Geophysical Research: Space Physics*, 104, 12313-12326. doi:  
608 10.1029/1999ja900089
- 609 Kieokaew, R., Lavraud, B., Fargette, N., Marchaudon, A., Génot, V., Jacquey, C.,  
610 ... Burch, J. (2021). Statistical relationship between interplanetary magnetic  
611 field conditions and the helicity sign of flux transfer event flux ropes. *Geophys-*  
612 *ical Research Letters*, 48(6), e2020GL091257. (e2020GL091257 2020GL091257)  
613 doi: <https://doi.org/10.1029/2020GL091257>
- 614 King, J. H., & Papitashvili, N. E. (2005). Solar wind spatial scales in and compar-  
615 isons of hourly wind and ace plasma and magnetic field data. *Journal of Geo-*  
616 *physical Research: Space Physics*, 110(A2). Retrieved from [https://agupubs](https://agupubs.onlinelibrary.wiley.com/doi/abs/10.1029/2004JA010649)  
617 [.onlinelibrary.wiley.com/doi/abs/10.1029/2004JA010649](https://agupubs.onlinelibrary.wiley.com/doi/abs/10.1029/2004JA010649) doi: [https://](https://doi.org/10.1029/2004JA010649)  
618 [doi.org/10.1029/2004JA010649](https://doi.org/10.1029/2004JA010649)
- 619 Lee, L. C., & Fu, Z. F. (1985). A theory of magnetic flux transfer at the earth's  
620 magnetopause. *Geophysical Research Letters*, 12(2), 105-108. doi: [https://doi](https://doi.org/10.1029/GL012i002p00105)  
621 [.org/10.1029/GL012i002p00105](https://doi.org/10.1029/GL012i002p00105)

- 622 Lepping, R. P., Jones, J. A., & Burlaga, L. F. (1990). Magnetic field structure of  
 623 interplanetary magnetic clouds at 1 au. *Journal of Geophysical Research*, *95*,  
 624 11957. doi: 10.1029/ja095ia08p11957
- 625 Lundquist, S. (1950). Magnetohydrostatic fields. *Arkiv För Fyzik*, *2*(35), 361-365.
- 626 Mandt, M. E., Denton, R. E., & Drake, J. F. (1994). Transition to whistler me-  
 627 diated magnetic reconnection. *Geophysical Research Letters*, *21*(1), 73-76.  
 628 Retrieved from [https://agupubs.onlinelibrary.wiley.com/doi/abs/](https://agupubs.onlinelibrary.wiley.com/doi/abs/10.1029/93GL03382)  
 629 [10.1029/93GL03382](https://doi.org/10.1029/93GL03382) doi: <https://doi.org/10.1029/93GL03382>
- 630 Mozer, F. S., & Hull, A. (2010). Scaling the energy conversion rate from magnetic  
 631 field reconnection to different bodies. *Physics of Plasmas*, *17*(10), 102906. Re-  
 632 trieved from <https://doi.org/10.1063/1.3504224> doi: 10.1063/1.3504224
- 633 Nagai, T., Shinohara, I., Fujimoto, M., Hoshino, M., Saito, Y., Machida, S., &  
 634 Mukai, T. (2001). Geotail observations of the hall current system: Evi-  
 635 dence of magnetic reconnection in the magnetotail. *Journal of Geophysical*  
 636 *Research: Space Physics*, *106*(A11), 25929-25949. Retrieved from [https://](https://agupubs.onlinelibrary.wiley.com/doi/abs/10.1029/2001JA900038)  
 637 [agupubs.onlinelibrary.wiley.com/doi/abs/10.1029/2001JA900038](https://agupubs.onlinelibrary.wiley.com/doi/abs/10.1029/2001JA900038) doi:  
 638 <https://doi.org/10.1029/2001JA900038>
- 639 Øieroset, M., Phan, T. D., Eastwood, J. P., Fujimoto, M., Daughton, W., Shay,  
 640 M. A., ... Glassmeier, K.-H. (2011, Oct). Direct evidence for a three-  
 641 dimensional magnetic flux rope flanked by two active magnetic reconnection  
 642  $x$  lines at earth's magnetopause. *Phys. Rev. Lett.*, *107*, 165007. Retrieved  
 643 from <https://link.aps.org/doi/10.1103/PhysRevLett.107.165007> doi:  
 644 [10.1103/PhysRevLett.107.165007](https://doi.org/10.1103/PhysRevLett.107.165007)
- 645 Paschmann, G., Haerendel, G., Papamastorakis, I., Sckopke, N., Bame, S. J.,  
 646 Gosling, J. T., & Russell, C. T. (1982). Plasma and magnetic field character-  
 647 istics of magnetic flux transfer events. *Journal of Geophysical Research: Space*  
 648 *Physics*, *87*(A4), 2159-2168. doi: <https://doi.org/10.1029/JA087iA04p02159>
- 649 Pollock, C., Moore, T., Jacques, A., Burch, J., Gliese, U., Saito, Y., ... Zeuch, M.  
 650 (2016). Fast Plasma Investigation for Magnetospheric Multiscale. *Space Sci-*  
 651 *ence Reviews*, *199*, 331-406. doi: <https://doi.org/10.1007/s11214-016-0245-4>
- 652 Raeder, J. (2006). Flux transfer events: 1. generation mechanism for strong south-  
 653 ward imf. *Annales Geophysicae*, *24*(1), 381-392. doi: [https://doi.org/10.5194/](https://doi.org/10.5194/angeo-24-381-2006)  
 654 [angeo-24-381-2006](https://doi.org/10.5194/angeo-24-381-2006)

- 655 Rijnbeek, R. P., Cowley, S. W. H., Southwood, D. J., & Russell, C. T. (1982).  
 656 Observations of reverse polarity flux transfer events at the earth's dayside  
 657 magnetopause. *Nature*, *300*, 23–26. doi: <https://doi.org/10.1038/300023a0>
- 658 Russell, C. T., Anderson, B. J., Baumjohann, W., Bromund, K. R., Dearborn, D.,  
 659 Fischer, D., ... Richter, I. (2016). The Magnetospheric Multiscale Magne-  
 660 tometers. *Space Science Reviews*, *199*, 189–256. doi: <https://doi.org/10.1007/s11214-014-0057-3>
- 662 Russell, C. T., & Elphic, R. C. (1978). Initial isee magnetometer results: magne-  
 663 topause observations. *Space Science Review*, *22*, 681–715. doi: <https://doi.org/10.1007/BF00212619>
- 665 Russell, C. T., & Elphic, R. C. (1979). Isee observations of flux transfer events at  
 666 the dayside magnetopause. *Geophysical Research Letters*, *6*(1), 33–36. doi:  
 667 <https://doi.org/10.1029/GL006i001p00033>
- 668 Rème, H., Bosqued, J. M., Sauvaud, J. A., Cros, A., Dandouras, J., Aoustin, C.,  
 669 ... Chionchio, G. (1997). The Cluster Ion Spectrometry Experiment. *Space*  
 670 *Science Reviews*, *78*, 303–350. doi: <https://doi.org/10.1023/A:1004929816409>
- 671 Saunders, M. A., Russell, C. T., & Sckopke, N. (1984). Flux transfer events: Scale  
 672 size and interior structure. *Geophysical Research Letters*, *11*(2), 131–134.  
 673 Retrieved from [https://agupubs.onlinelibrary.wiley.com/doi/abs/](https://agupubs.onlinelibrary.wiley.com/doi/abs/10.1029/GL011i002p00131)  
 674 [10.1029/GL011i002p00131](https://doi.org/10.1029/GL011i002p00131) doi: <https://doi.org/10.1029/GL011i002p00131>
- 675 Scholer, M. (1988). Magnetic flux transfer at the magnetopause based on single  
 676 x line bursty reconnection. *Geophysical Research Letters*, *15*(4), 291–294.  
 677 Retrieved from [https://agupubs.onlinelibrary.wiley.com/doi/abs/](https://agupubs.onlinelibrary.wiley.com/doi/abs/10.1029/GL015i004p00291)  
 678 [10.1029/GL015i004p00291](https://doi.org/10.1029/GL015i004p00291) doi: <https://doi.org/10.1029/GL015i004p00291>
- 679 Shue, J.-H., Song, P., Russell, C. T., Steinberg, J. T., Chao, J. K., Zastenker, G., ...  
 680 Kawano, H. (1998). Magnetopause location under extreme solar wind condi-  
 681 tions. *Journal of Geophysical Research: Space Physics*, *103*(A8), 17691–17700.  
 682 doi: <https://doi.org/10.1029/98JA01103>
- 683 Southwood, D., Farrugia, C., & Saunders, M. (1988). What are flux trans-  
 684 fer events? *Planetary and Space Science*, *36*(5), 503–508. Retrieved from  
 685 <https://www.sciencedirect.com/science/article/pii/0032063388901092>  
 686 doi: [https://doi.org/10.1016/0032-0633\(88\)90109-2](https://doi.org/10.1016/0032-0633(88)90109-2)
- 687 Teh, W. L., Abdullah, M., & Hasbi, A. M. (2014). Evidence for the core

688 field polarity of magnetic flux ropes against the reconnection guide field.

689 *Journal of Geophysical Research: Space Physics*, 119, 8979-8983. doi:

690 10.1002/2014JA020509

691 Teh, W.-L., Nakamura, R., Karimabadi, H., Baumjohann, W., & Zhang, T. L.

692 (2014). Correlation of core field polarity of magnetotail flux ropes with

693 the imf by: Reconnection guide field dependency. *Journal of Geophysi-*

694 *cal Research: Space Physics*, 119(4), 2933-2944. Retrieved from [https://](https://agupubs.onlinelibrary.wiley.com/doi/abs/10.1002/2013JA019454)

695 [agupubs.onlinelibrary.wiley.com/doi/abs/10.1002/2013JA019454](https://agupubs.onlinelibrary.wiley.com/doi/abs/10.1002/2013JA019454) doi:

696 <https://doi.org/10.1002/2013JA019454>

697 Trattner, K. J., Mulcock, J. S., Petrinec, S. M., & Fuselier, S. A. (2007). Location

698 of the reconnection line at the magnetopause during southward imf condi-

699 tions. *Geophysical Research Letters*, 34(3). doi: [https://doi.org/10.1029/](https://doi.org/10.1029/2006GL028397)

700 2006GL028397

701 Zhang, Y. C., Lavraud, B., Dai, L., Wang, C., Marchaudon, A., Avanov, L.,

702 ... Torbert, R. (2017). Quantitative analysis of a hall system in the

703 exhaust of asymmetric magnetic reconnection. *Journal of Geophysical*

704 *Research: Space Physics*, 122(5), 5277-5289. Retrieved from [https://](https://agupubs.onlinelibrary.wiley.com/doi/abs/10.1002/2016JA023620)

705 [agupubs.onlinelibrary.wiley.com/doi/abs/10.1002/2016JA023620](https://agupubs.onlinelibrary.wiley.com/doi/abs/10.1002/2016JA023620) doi:

706 <https://doi.org/10.1002/2016JA023620>

# The Helicity Sign of Flux Transfer Event Flux Ropes and its Relationship to the Guide Field and Hall Physics in Magnetic Reconnection at the Magnetopause

S. Dahani <sup>1</sup>, R. Kieokaew <sup>1</sup>, V. Génot <sup>1</sup>, B. Lavraud <sup>1,2</sup>, Y. Chen <sup>3</sup>, B.

Michotte de Welle <sup>4</sup>, N. Aunai <sup>4</sup>, G. Tóth <sup>5</sup>, P. A. Cassak <sup>6</sup>, N. Fargette <sup>1</sup>, R.

C. Fear <sup>7</sup>, A. Marchaudon <sup>1</sup>, D. Gershman <sup>8</sup>, B. Giles <sup>8</sup>, R. Torbert <sup>9</sup>, J.

Burch <sup>10</sup>

<sup>1</sup>Institut de Recherche en Astrophysique et Planétologie, CNRS, UPS, CNES, Université de Toulouse, Toulouse, France

<sup>2</sup>Laboratoire d'Astrophysique de Bordeaux, Univ. Bordeaux, CNRS, Pessac, France

<sup>3</sup>Department of Astrophysical Sciences and Princeton Plasma Physics Laboratory, Princeton University, Princeton, NJ 08540, USA

<sup>4</sup>Laboratory of Plasma Physics, CNRS, Ecole Polytechnique, UPMC, Université Paris Sud, Orsay, France

<sup>5</sup>Department of Climate and Space Sciences and Engineering, University of Michigan, Ann Arbor, MI, USA

<sup>6</sup>Department of Physics and Astronomy and center for KINETIC Plasma Physics, West Virginia University, Morgantown, WV, USA

<sup>7</sup>Department of Physics & Astronomy, University of Southampton, Southampton, UK

<sup>8</sup>NASA Goddard Space Flight Center, Greenbelt, MD, USA

<sup>9</sup>Space Science Center, University of New Hampshire, Durham, NH, USA

<sup>10</sup>Southwest Research Institute, San Antonio, TX, USA

## Contents of this file

1. Table S1

---

**Introduction** This supplementary information includes Table S1 which lists the 82 events observed by the Cluster spacecraft. Events from Magnetospheric Multiscale are found in the supplementary information of Kieokaew et al. (2021). Table S1 includes the spacecraft used to observe the FTE where c1 denotes Cluster 1 and c3 denotes Cluster 3, the start and end times of the observation, which correspond to the start and end of the bipolar variation, the location in the Geocentric Solar Ecliptic (GSE) coordinate system and the helicity sign  $H$ .

s/c	tbegin	tend	X_GSE	Y_GSE	Z_GSE	H
c1	2002-11-10T10:15:40.000	2002-11-10T10:16:00.000	-5.477	16.818	-5.114	-1
c1	2002-11-10T10:17:45.000	2002-11-10T10:18:35.313	-5.663	17.4	-5.232	-1
c1	2002-11-10T10:44:46.000	2002-11-10T10:45:30.000	-5.297	16.694	-5.371	-1
c1	2002-11-10T10:53:47.000	2002-11-10T10:54:30.588	-5.466	17.263	-5.536	-1
c1	2002-11-10T11:42:15.000	2002-11-10T11:43:30.000	-5.188	17.046	-5.94	-1
c1	2002-11-10T11:59:44.940	2002-11-10T12:00:19.609	-4.813	16.314	-6.017	1
c1	2002-11-10T12:49:00.000	2002-11-10T12:50:30.608	-4.797	16.7	-6.465	1
c1	2002-11-10T13:01:28.000	2002-11-10T13:03:02.352	-4.718	16.625	-6.565	1
c1	2002-11-12T10:29:00.000	2002-11-12T10:29:46.710	-7.271	17.226	0.039	-1
c1	2002-11-12T10:58:30.000	2002-11-12T10:59:45.952	-7.171	17.325	-0.264	1
c1	2002-11-12T11:08:50.000	2002-11-12T11:09:17.135	-7.136	17.355	-0.365	1
c1	2002-11-12T13:10:40.000	2002-11-12T13:12:00.000	-6.669	17.604	-1.581	-1
c1	2002-11-12T13:53:00.000	2002-11-12T13:54:00.021	-6.484	17.641	-2.01	-1
c3	2002-11-12T19:06:47.000	2002-11-12T19:07:17.740	-5.017	17.685	-5.104	1
c1	2002-11-12T20:45:30.000	2002-11-12T20:46:30.000	-4.249	16.618	-5.864	-1
c1	2002-11-12T20:53:30.000	2002-11-12T20:54:02.000	-4.198	16.573	-5.932	1
c1	2002-11-12T21:45:45.000	2002-11-12T21:47:15.684	-4.143	16.943	-6.41	-1
c3	2002-11-13T00:04:30.000	2002-11-13T00:05:45.359	-2.923	15.191	-7.435	1
c3	2002-11-13T00:08:30.000	2002-11-13T00:09:28.000	-3.289	15.965	-7.46	1
c1	2002-11-13T00:25:15.000	2002-11-13T00:26:30.000	-3.183	15.828	-7.576	1
c1	2002-11-15T01:20:00.000	2002-11-15T01:21:30.159	-5.061	17.801	-3.421	1
c1	2002-11-15T01:27:30.000	2002-11-15T01:29:00.000	-5.057	18.304	-3.66	1
c1	2002-11-15T02:14:15.000	2002-11-15T02:16:00.000	-4.849	18.225	-4.077	1
c1	2002-11-15T04:31:30.000	2002-11-15T04:32:00.000	-4.027	17.201	-5.186	-1
c1	2002-11-15T11:06:00.000	2002-11-15T11:07:02.000	-1.511	14.135	-8.226	1
c1	2002-11-17T04:32:00.000	2002-11-17T04:33:00.000	-5.806	17.769	0.023	-1
c1	2002-11-17T05:21:00.000	2002-11-17T05:21:40.640	-5.654	17.893	-0.401	-1
c1	2002-11-17T05:23:30.108	2002-11-17T05:24:00.143	-5.646	17.898	-0.421	-1
c1	2002-11-17T05:31:10.326	2002-11-17T05:31:40.241	-5.616	17.919	-0.502	-1
c1	2002-11-17T05:37:10.000	2002-11-17T05:37:40.000	-5.594	17.933	-0.562	-1

c1	2002-11-17T05:51:15.000	2002-11-17T05:52:00.000	-5.54	17.965	-0.703	-1
c1	2002-11-17T23:24:27.712	2002-11-17T23:25:00.000	0.296	11.656	-9.19	-1
c3	2002-11-26T13:54:30.000	2002-11-26T13:55:10.000	-3.131	18.034	1.488	1
c1	2002-11-28T18:46:15.000	2002-11-28T18:47:30.000	-3.563	15.925	4.317	1
c3	2002-11-28T19:48:30.000	2002-11-28T19:50:00.000	-2.955	16.751	3.269	1
c1	2002-12-01T04:11:29.000	2002-12-01T04:12:30.000	-2.822	16.246	4.131	1
c1	2002-12-08T03:53:40.000	2002-12-08T03:54:28.409	-1.676	14.166	5.957	-1
c1	2002-12-08T05:51:48.000	2002-12-08T05:52:50.000	-1.185	15.555	4.988	-1
c3	2002-12-08T06:13:50.712	2002-12-08T06:15:30.000	-0.602	15.93	4.294	-1
c3	2002-12-08T08:45:55.000	2002-12-08T08:46:40.000	0.034	17.306	2.94	-1
c1	2002-12-10T15:27:45.727	2002-12-10T15:30:00.000	-0.384	15.913	4.689	-1
c1	2002-12-10T15:59:33.986	2002-12-10T16:01:00.000	0.241	16.326	3.935	1
c1	2002-12-10T16:48:56.000	2002-12-10T16:50:05.501	0.003	16.642	3.96	-1
c1	2002-12-10T22:48:00.000	2002-12-10T22:49:33.000	1.716	18.515	0.446	-1
c1	2002-12-24T16:10:17.254	2002-12-24T16:10:57.690	0.869	11.273	7.284	-1
c3	2003-01-07T21:43:30.000	2003-01-07T21:44:00.000	3.282	9.511	6.992	-1
c3	2003-01-07T21:50:30.594	2003-01-07T21:51:45.000	3.386	9.636	6.958	-1
c1	2003-01-10T05:35:43.607	2003-01-10T05:36:33.381	2.317	8.546	7.78	-1
c1	2003-01-10T05:49:15.000	2003-01-10T05:50:45.000	2.837	8.378	7.19	1
c1	2003-01-10T06:07:25.875	2003-01-10T06:07:50.762	2.495	8.76	7.744	-1
c3	2003-01-15T01:25:15.000	2003-01-15T01:25:51.416	4.833	9.355	6.866	-1
c3	2003-01-15T01:45:45.000	2003-01-15T01:46:15.000	5.137	9.63	6.763	-1
c3	2003-01-15T01:50:50.000	2003-01-15T01:52:30.000	5.194	9.693	6.738	-1
c3	2003-01-15T02:11:33.108	2003-01-15T02:12:30.000	5.505	9.954	6.626	-1
c3	2003-01-15T03:14:10.000	2003-01-15T03:14:30.000	6.347	10.661	6.255	-1
c1	2003-01-22T04:45:08.000	2003-01-22T04:45:30.000	5.647	9.089	7.377	1
c1	2003-01-31T19:27:26.000	2003-01-31T19:28:00.000	9.329	8.97	6.51	-1
c1	2003-01-31T19:43:45.000	2003-01-31T19:44:45.000	9.577	9.061	6.39	1
c3	2003-02-02T23:35:56.000	2003-02-02T23:36:53.000	4.412	6.285	7.817	1
c1	2003-02-03T00:37:45.000	2003-02-03T00:38:45.000	5.646	6.92	7.698	1
c3	2003-02-03T01:04:25.000	2003-02-03T01:04:52.000	6.304	6.679	7.062	1
c3	2003-02-07T18:33:15.000	2003-02-07T18:34:00.000	5.898	5.738	7.146	-1
c1	2003-02-07T20:51:20.000	2003-02-07T20:54:00.000	8.671	6.73	6.617	1
c1	2003-02-17T07:25:00.000	2003-02-17T07:26:30.000	7.393	4.82	7.043	1
c3	2003-02-22T02:00:00.000	2003-02-22T02:01:15.000	8.246	4.217	6.943	1
c1	2003-03-05T21:14:30.000	2003-03-05T21:15:30.000	5.916	3.104	7.675	-1
c1	2003-03-08T07:02:53.000	2003-03-08T07:03:36.000	7.086	2.761	7.656	-1
c1	2003-03-15T09:22:15.000	2003-03-15T09:22:55.000	5.97	2.143	7.638	1
c1	2003-03-15T09:48:43.000	2003-03-15T09:49:14.000	6.633	2.019	7.653	1
c3	2003-03-15T09:53:55.000	2003-03-15T09:55:00.000	6.393	1.569	7.052	1
c3	2003-03-19T13:57:30.000	2003-03-19T13:58:30.000	2.07	-4.567	-9.129	1
c1	2003-04-08T03:42:15.000	2003-04-08T03:43:30.000	5.403	0.085	7.469	1
c1	2003-04-20T02:37:56.000	2003-04-20T02:38:57.000	6.846	-2.619	7.518	1

May 27, 2022, 1:13pm

c3	2003-04-24T22:00:00.000	2003-04-24T22:00:45.000	7.617	-4.482	7.364	-1
c3	2003-05-28T04:09:24.000	2003-05-28T04:09:50.000	3.347	-6.063	6.834	-1
c3	2003-06-03T09:56:23.000	2003-06-03T09:58:00.000	-3.552	-12.872	-9.585	-1
c3	2003-06-03T12:40:00.000	2003-06-03T12:41:03.000	-3.769	-10.416	-10.028	1
c1	2003-06-05T13:29:08.000	2003-06-05T13:29:45.000	-3.426	-15.557	-7.94	1
c1	2003-06-19T16:10:22.000	2003-06-19T16:11:45.000	-6.778	-16.569	-6.032	-1
c1	2003-06-23T17:16:53.000	2003-06-23T17:17:45.000	-3.478	-15.412	4.271	-1
c1	2003-06-27T03:26:45.000	2003-06-27T03:28:45.000	-8.432	-11.976	-8.773	-1
c1	2003-06-27T03:38:05.000	2003-06-27T03:39:10.000	-8.411	-11.866	-8.823	1

## References

Kieokaew, R., Lavraud, B., Fargette, N., Marchaudon, A., Génot, V., Jacquy, C., ... Burch, J. (2021). Statistical relationship between interplanetary magnetic field conditions and the helicity sign of flux transfer event flux ropes. *Geophysical Research Letters*, 48(6), e2020GL091257. (e2020GL091257 2020GL091257) doi: <https://doi.org/10.1029/2020GL091257>